

Earth and Space Science



RESEARCH ARTICLE

10.1029/2019EA000992

Special Section:
InSight at Mars

Key Points:

- Solar array current telemetry gives situational awareness of the Mars surface environment
- Dust in the atmosphere is observed to vary
- Twilight currents indicate clouds

Correspondence to:

R. D. Lorenz,
ralph.lorenz@jhuapl.edu

Citation:

Lorenz, R. D., Lemmon, M. T., Maki, J., Banfield, D., Spiga, A., Charalambous, C., et al. (2020). Scientific observations with the InSight solar arrays: Dust, clouds, and eclipses on Mars. *Earth and Space Science*, 7, e2019EA000992. <https://doi.org/10.1029/2019EA000992>

Received 11 NOV 2019

Accepted 1 APR 2020

Accepted article online 14 APR 2020

Scientific Observations With the InSight Solar Arrays: Dust, Clouds, and Eclipses on Mars

Ralph D. Lorenz¹ , Mark T. Lemmon² , Justin Maki³ , Donald Banfield⁴ , Aymeric Spiga^{5,6} , Constantinos Charalambous⁷ , Elizabeth Barrett³, Jennifer A. Herman³ , Brett T. White⁸, Samuel Pasco⁸, and W. Bruce Banerdt³ 

¹Johns Hopkins Applied Physics Laboratory, Laurel, MD, USA, ²Space Science Institute, College Station, TX, USA, ³Jet Propulsion Laboratory, California Institute of Technology, Pasadena, CA, USA, ⁴Cornell Center for Astrophysics and Planetary Science, Ithaca, NY, USA, ⁵Laboratoire de Météorologie Dynamique (LMD/IPSL), Sorbonne Université, Centre National de la Recherche Scientifique, École Polytechnique, École Normale Supérieure, Paris, France, ⁶Institut Universitaire de France, Paris, France, ⁷Department of Electrical and Electronic Engineering, Imperial College, South Kensington Campus, London, UK, ⁸Lockheed Martin Space, Littleton, CO, USA

Abstract Records of solar array currents recorded by the InSight lander during its first 200 sols on Mars are presented. In addition to the geometric variation in illumination on seasonal and diurnal timescales, the data are influenced by dust suspended in the atmosphere and deposited on the solar panels. Although no dust devils have been detected by InSight's cameras, brief excursions in solar array currents suggest that at least some of the vortices detected by transient pressure drops are accompanied by dust. A step increase in array output (i.e., a "cleaning event") was observed to be directly associated with the passage of a strong vortex. Some quasiperiodic variations in solar array current are suggestive of dust variations in the planetary boundary layer. Nonzero array outputs before sunrise and after sunset are indicative of scattering in the atmosphere: A notable increase in evening twilight currents is observed associated with noctilucent clouds, likely of water or carbon dioxide ice. Finally, although the observations are intermittent (typically a few hours per sol) and at a modest sample rate (one to two samples per minute), three single-sample light dips are seen associated with Phobos eclipses. These results demonstrate that engineering data from solar arrays provide valuable scientific situational awareness of the Martian environment.

1. Introduction

Although solar array performance data have been obtained for engineering operations during previous landed Mars missions, these data have not in general been made publicly available in electronic form. The InSight mission, however, has included such data in the public archive, since the solar array currents have a direct and prominent influence on the scientific instrumentation (notably, the seismometer and magnetometer). It may be noted that the InSight solar arrays (Figure 1) with an active area of some 5.14 m² are in fact the largest and most powerful ever deployed on the Red Planet (e.g., Lisano & Kallemeyn, 2017; Lam et al., 2016), able to produce some 4 kWh of energy per Martian day (sol).

The current data from these arrays provide a useful window on the Martian environment that can be exploited for scientific purposes, supplementing the dedicated atmospheric science payload on InSight (e.g., Spiga et al., 2018). On previous missions, the engineering performance of solar arrays has been reported (e.g., for Pathfinder/Sojourner, Landis, 1996; Crisp et al., 2004; for Phoenix, Coyne et al., 2009; for the Mars Exploration Rovers, Stella et al., 2008, 2009), but after the initial report of dust settling on Sojourner, the environmental insights afforded by solar array data have received relatively little comment, although see Lorenz and Jackson (2015) for the potential of similar data at Mars analog sites on Earth.

The InSight mission is ongoing: The present report reviews the findings from solar array current data acquired from landing (26 November 2018; Julian Date 2458449, Mars solar longitude $L_s = 295.5^\circ$, Mars Year 34, Sol 555) to InSight Sol 200 (19 June 2019; Julian Date 2458654, $L_s = 41.4^\circ$, Mars Year 35, Sol 77).

2. Data

The InSight seismometer's exquisite sensitivity means that changes in electrical power supply conditions could introduce spurious signals. Similarly, there is a small susceptibility to changing magnetic fields.

©2020. The Authors.

This is an open access article under the terms of the Creative Commons Attribution-NonCommercial-NoDerivs License, which permits use and distribution in any medium, provided the original work is properly cited, the use is non-commercial and no modifications or adaptations are made.

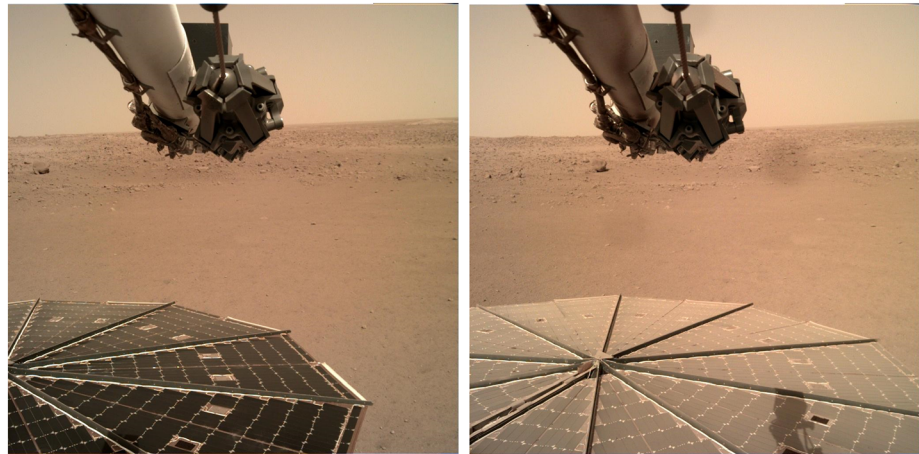


Figure 1. InSight solar arrays on the surface of Mars on (left) Sol 14 and (right) Sol 100. The dust accumulation between the image acquisitions is evident. Notice the shadow of the robotic arm on the Sol 100 image—see section 7. A smudge-like blemish in the Sol 100 image, just to the right of the grapple, is a dust mote on the camera window. Image data set identifiers are D012R0014_597777297EDR_F0103_0100M and D014R0100_605416417EDR_F0103_0100M.

InSight was therefore equipped with a magnetometer to allow the identification of any magnetic perturbations. Some of the local magnetic field is caused by the currents flowing in the arrays and the cables to and from the lander, so these currents are recorded and archived. The InSight Fluxgate Magnetometer (IFG) data archived on the NASA Planetary Data System (PDS) Planetary Plasma Interactions Node (<https://pds-ppi.igpp.ucla.edu>) include solar array current data in the InSight Spacecraft Raw Engineering and Ancillary Data Collection (e.g., the Sol 91 data are data set **ancil_SOL0091_20190227_20190228_v01.tab**). Only two of the telemetry channels are straightforward to relate the Martian surface environment. These are E-0771 (Array 1, +Y, East) and E-0791 (Array 2, -Y, West), which correspond to “hardwired” strings of the solar arrays that are connected directly to the battery.

These hardwired strings (for “Dead Bus Recovery” [DBR]; Lam et al., 2016) are located on the perimeter of the arrays. Other telemetry channels record certain other currents, but these depend on the battery state of charge and on the varying spacecraft loads and so are not as straightforward to interpret in terms of the Mars environment.

The physics of photodiodes such as solar cells is such that in a short-circuit condition, the photocurrent is linearly related to the light flux incident onto the semiconductor. Although the open-circuit voltage of a cell has a substantial dependence on temperature, the short-circuit current does not (e.g., a typical silicon cell may have its current increase by only 0.02% if it warms from 20 to 90 °C, while the open-circuit voltage may decrease by 20%.) We have therefore made no attempt to normalize results to a reference temperature. The current and voltage characteristics of solar cells on Mars are discussed in some detail by Crisp et al. (2004).

In high-efficiency triple-junction cells such as those used on InSight (Lam et al., 2016), the current output will be the minimum of the three stacked semiconductor layers that each intercept a different part of the solar spectrum. If the incident spectrum is changed significantly (e.g., the light becomes significantly reddened by a dust storm), the proportionality of current to total flux may change, in that the output may become current limited by the blue-absorbing semiconductor layer rather than the red-absorbing layer (see, e.g., Stella et al., 2008). Thus, some caution should be exercised in attempting any type of absolute radiometric analysis, especially if the spectrum may be variable. However, here we are

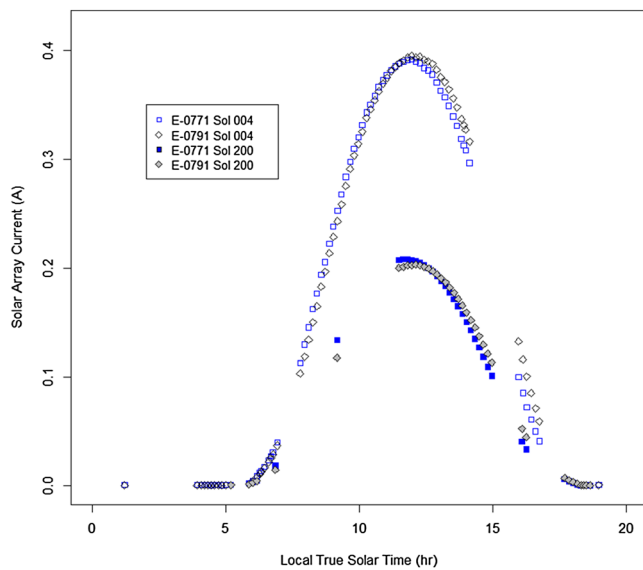


Figure 2. Example data from Sols 4 and 200. Note that the currents are a factor of 2 lower on Sol 200. Note that the E-0771 currents are slightly higher in the morning, while the E-0791 are slightly higher in the afternoon, possibly indicating some array tilt or different reflection or shadowing by lander structures. Data have been decimated to avoid overplotting symbols: Data for 20:00–24:00 h, not shown, are similar to 00:00–05:00 h, that is, zero with extended gaps.

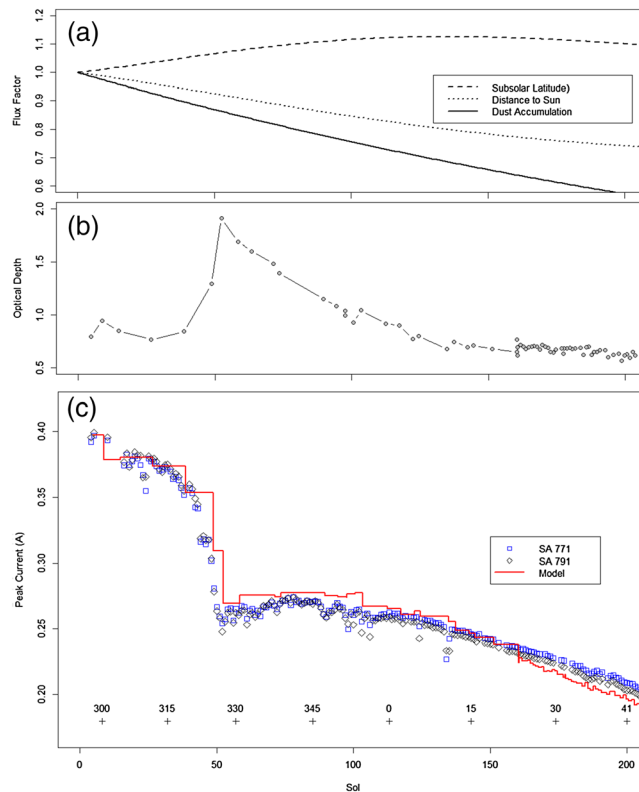


Figure 3. (a) Lines show three multiplicative factors driving the evolution of the peak (noon) current from InSight’s arrays. The dashed black line shows the effect of solar latitude, while the dotted line shows the inverse square impact of changing solar distance. The solid line shows the assumed effect of dust accumulation on the array, leading to a progressive 0.28%/sol loss. (b) The optical depth of suspended dust, measured from lander images (these determinations were made more frequently as the mission went on). (c) The maximum recorded current per sol for the two arrays (black diamonds, SA791; blue squares, SA771)—occasional short “dips” are simply because measurements were not acquired at noon. The solid red staircase line is a simple model with the latitude and distance effect combined with a $(1/[1 + 0.3\tau])$ factor (the steps corresponding to updated τ values) and a 0.28%/sol assumed loss due to dust deposition on the arrays.

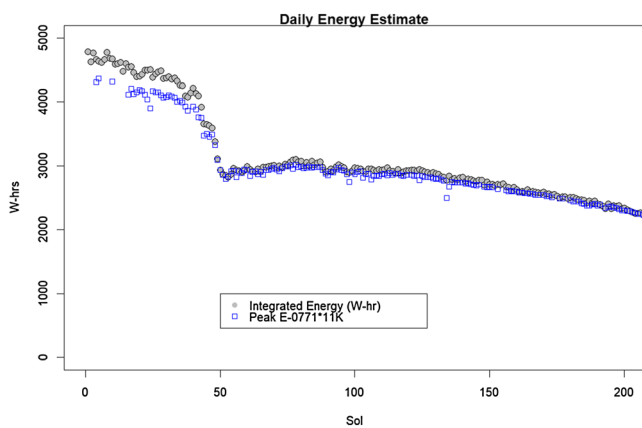


Figure 4. Daily operational total energy estimated from an analytic fit to array current and voltage telemetry. Apart from a low bias at the beginning of the mission (perhaps due to the arrays being relatively clear of dust), and a few spurious drops where data were not taken close to noon, a simple multiplication of the peak current (A) by 11,000 Vh yields a good heuristic estimate of the total energy production.

concerned primarily with simple time variations where such complications are unimportant.

The response of solar cells to flux as a function of incident angle depends slightly on the refractive index of the cells or cover glass due to Fresnel reflection. However, except at very low (grazing) influence is only a few percent (see, e.g., Crisp et al., 2004), and again in the present paper we are concerned only with temporal changes.

The DBR circuit on each array comprises four strings of 15 cells in series, each cell with an open-circuit voltage of 2.258 V—see Lam et al. (2016). The direct connection of these strings (with a voltage rather higher than the battery voltage of 28 V) approximates a short-circuit arrangement, making the current in these telemetry channels directly proportional to the light flux. The array currents are not recorded continuously, but only when the lander is in an “awake” state, for example, when transmitting data to an orbiter. Thus, extensive gaps in the record often occur, when the lander is “off” for several hours at a time to minimize its energy usage: A

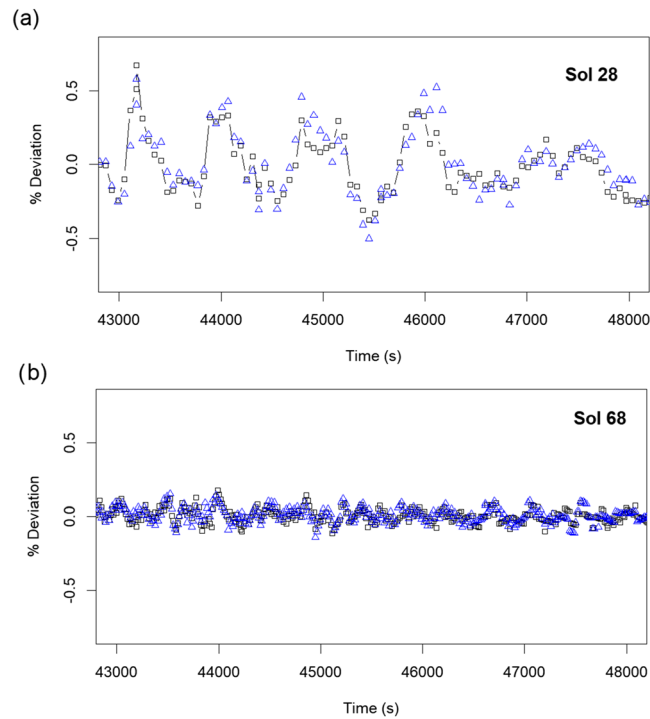


Figure 5. Short-term variations in solar flux near local noon. A 20-point running mean is subtracted from the instantaneous currents (black squares, SA771; blue triangles, SA791), and the residual is expressed as a percentage. (a) In early sols, there is a quasiperiodic variation with a peak-to-peak amplitude of ~1% and a period of about 1,000 s. The coherent (point-to-point) trajectory of the data and the correspondence between the two channels indicate this to be a real environmental effect. (b) Later in the mission, these variations were much smaller.

typical record is illustrated in Figure 2. When the lander is awake, the array currents are recorded at intervals of typically 30 or 60 s, a cadence chosen as yielding adequate insight into the performance of the arrays for operations planning, while not demanding too high a data volume.

ASCII tables of the E-0771 and E-0791 engineering telemetry channels (sometimes referred to as SA-0771 or SAC-0771, etc., to indicate their function as solar array currents), with timing information, are made available on the Applied Physics Lab data archive (<http://lib.jhuapl.edu>).

As might be expected, the diurnal record has a positive sine shape during the day, since the lander is at low latitude with horizontal arrays, and so the current varies roughly with the sine of solar elevation, while being zero at night. Deviations from this pattern are discussed in later sections.

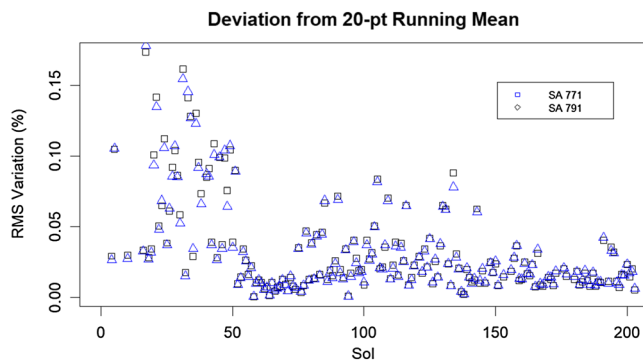


Figure 6. Root-mean-square deviation (roughly, the amplitude of variations like those in Figure 4) from a smooth profile throughout the mission. The deviations were strongest in the first 50 sols and then declined.

3. Long-Term Variations

Three principal factors influence the solar array output at a fixed station on a flat area of Mars over multi-sol timescales (the more complicated situation where terrain causes shadows has been recently assessed by Spagnuolo et al., 2019). First is the astronomical (seasonal) variation, due to the changing track of the Sun across the sky, and the changing Mars-Sun distance. At InSight's low latitude (4.502°N , Banerdt et al., 2020), there is relatively little length-of-day variation and a modest ($1 - \cos[\text{obliquity}] \sim 10\%$) change in projected flux due to noontime solar elevation. Thus, the predominant astronomical effect is due to the heliocentric eccentricity of the Martian orbit, such that the Mars-Sun

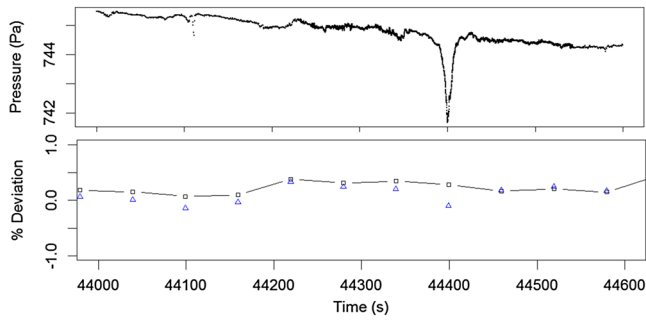


Figure 7. A possible dust devil shadow occurred on Sol 26 at 44,400 s, where a drop in SA-0791 current of about 0.3% occurred, coincident with the pressure drop typical of convective vortices.

distance grows steadily from 1.41 AU on Sol 1 to 1.62 AU on Sol 200—see Figure 3.

The second effect is the amount of dust suspended in the atmosphere, usually expressed as a vertical column-integrated optical depth (“tau”). This has been measured at intervals of typically a few sols from measurements of near-Sun sky brightness from the imagers on InSight (Spiga et al., 2018), as on previous Mars missions (e.g., Lemmon et al., 2015). The initial value was around 0.7, but this grew dramatically over Sols 40–60 to a peak of 1.9 associated with a large dust storm and then declined back to a near steady state of 0.7 or so—see Banfield et al. (2020) and Lisano and Bernard (2014).

The dust is not black (i.e., exclusively absorbing), and thus, the effect of this partly scattering dust opacity is not a simple exponential attenuation.

Important prior discussions of the impact of suspended dust on Mars surface solar power include those by Crisp et al. (2004) and a particularly useful document by Rapp (2004). Over the range of $0.1 < \tau < 5$, we find that the numerical simulations of the flux attenuation at normal incidence by Crisp et al. (2004) can be approximated to a couple of percent by the very simple factor $1/(1 + 0.3\tau)$, where τ is the optical depth. Note that the simulations by Crisp et al. (2004) assumed the spectral response of a gallium arsenide/germanium double-junction cell, which is almost certainly somewhat different from that of

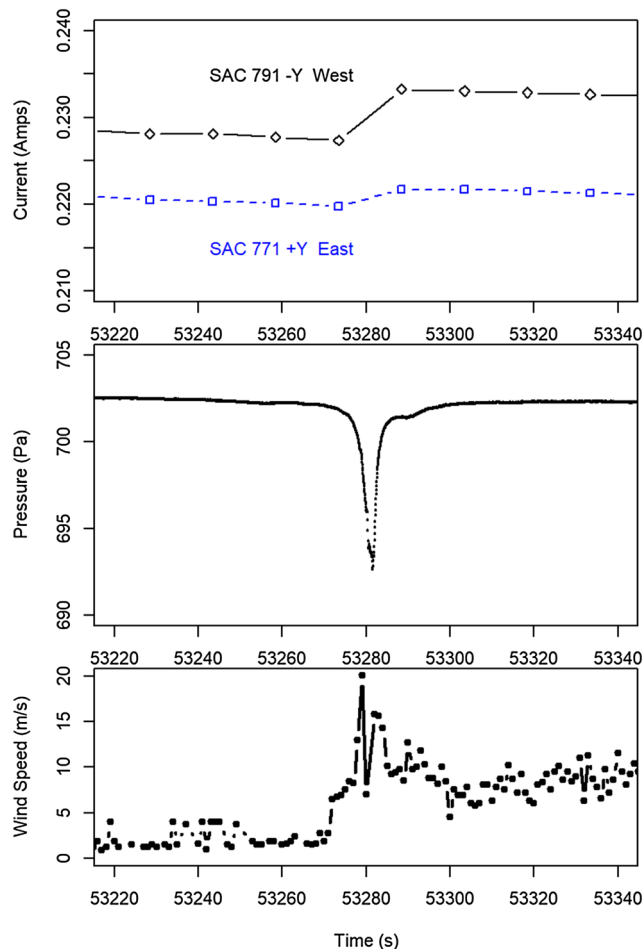


Figure 8. A 2.5-min segment of InSight data around the dust-cleaning event (centered on 14:51:58 UTC on Sol 65). Note that there is a data gap in the wind data in the middle of the event.

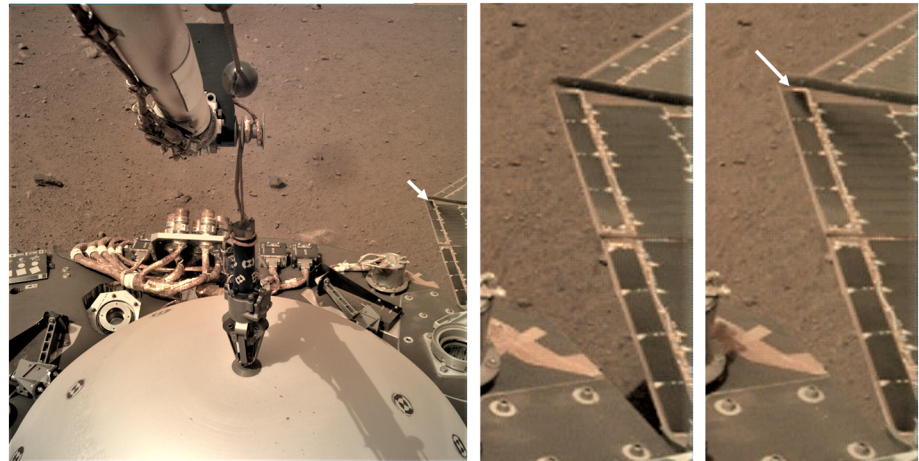


Figure 9. (left) Image acquired on Sol 65, 14:58 UTC (13:38 LTST) by the Instrument Deployment Camera (IDC) after capture of the Wind and Thermal Shield by the grapple. This image was taken approximately 6 min after the 9-Pa vortex occurred. The white arrow points to an elongated dark streak feature due to the dust-cleaning event on the west solar panel by the vortex. Enlarged and sharpened images of the west solar panel (middle) before and (right) after the 9-Pa vortex. The before image was captured by the IDC on Sol 65, 13:52 UTC (12:34 LTST), approximately 1 h before the vortex encounter and shows a uniform layer of dust on the panel, while the latter is a cropped and enlarged version of the left image indicating the dark area that has been cleared of dust, apparently in the lee of one of the ribs supporting the array.

InSight's triple-junction cells. However, the rather good match to the InSight data (Figure 3) shows that this nicely simple function does a reasonable job of predicting the current loss during the dust storm when tau rose significantly.

The final effect is the accumulation of airfall dust on the solar arrays, which also afflicts terrestrial solar power (e.g., Sayyah et al., 2014). This process likely varies with time and indeed is occasionally reversed

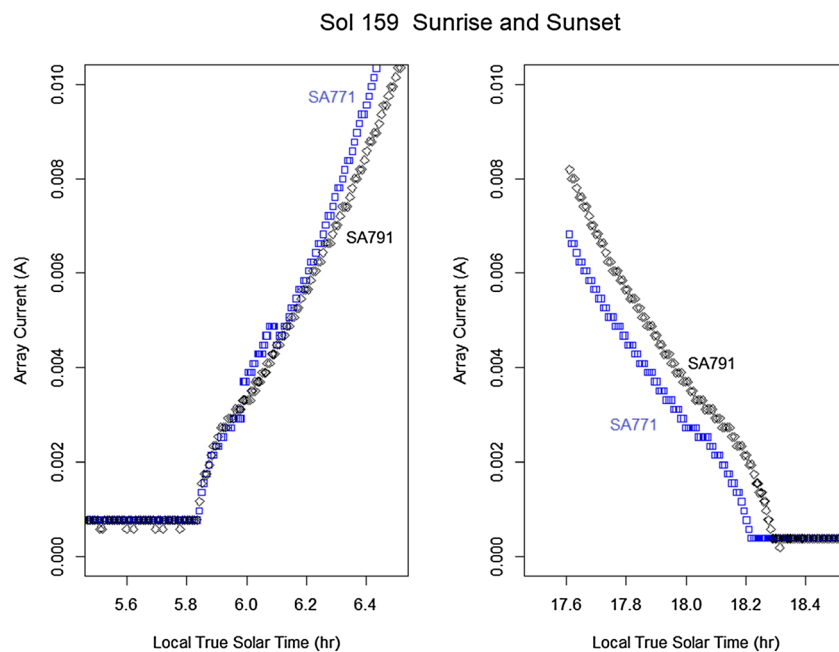


Figure 10. Array currents at sunrise and sunset on Sol 159. Note that the SA771 currents rise a little faster than the SA791 currents but then fall off faster. This is presumably due to shadowing effects of the lander structure and/or a slight tilt of the lander and/or the arrays—SA791, in particular, appears to have a tilt-driven bias at sunset. A “shoulder” to the curves is present at both sunrise and sunset due to atmospheric scattering but is more prominent at sunset.

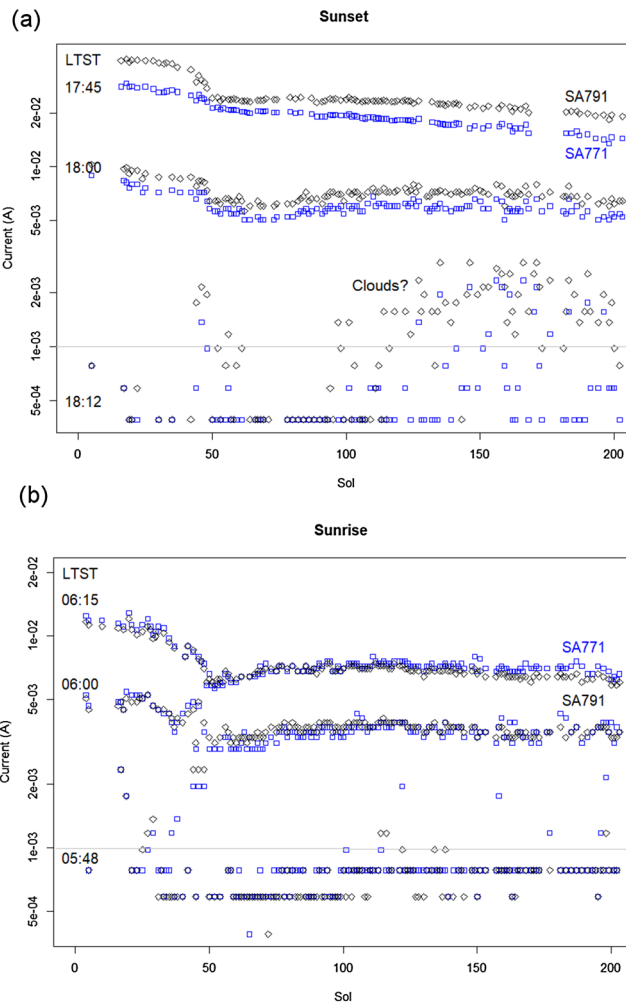


Figure 11. (a) Evolution of sunset currents throughout the mission. At LTST 17:45, the evolution mirrors that of the peak (noontime) current as in Figure 3. At 18:00, with the Sun on the horizon, the pattern is similar (e.g., with the decline around Sol 50 due to the dust storm) but in fact increases a little after Sol 70. The variability appears to increase somewhat too after Sol 150. At 18:12 h, with the Sun 3° below the horizon, there is essentially zero current for the first 100 sols, except for a few glimmers around Sol 50, perhaps linked to the dust storm. After Sol 100, frequent detections of light at 18:12 occur, presumably due to the presence of clouds. This pattern is not seen in (b) the corresponding sunrise data. Note that not all sols have data at these times—data are only shown when they exist within 1 min of the stated times. The gray line indicates a notional cloud detection threshold. Note that the ordinate scale is logarithmic.

by dust removal by vortices or gusts, but a steady state accumulation causing a drop in peak output of 0.28%/sol, as observed on the Sojourner solar arrays (Landis, 1996), appears to reproduce the observed power history (Figure 3). In project operations discussions, the obscuration is simply expressed as a multiplicative “array factor” or “dust factor,” the fraction of the output of a dust-free array that is being generated (see, e.g., Lorenz & Reiss, 2015; Stella et al., 2008). After 200 sols, the array factor would be expected to be $0.9972^{200}=57\%$.

It seems evident from Figure 3 that the combination of astronomical, atmospheric dust and expected array factors reproduces the observed history on InSight quite well. The sharp drop around Sol 50 and the partial recovery thereafter are due principally to suspended dust. Deposition on (and removal from) the arrays is a less prominent factor, albeit a slowly inevitable one. Further exploration of the relationship of dust devil activity with respect to the overall atmospheric opacity will be interesting. See also section 4. Crisp et al. (2004) observed on Mars Pathfinder (MPF), “Before sol 20, the power losses associated with dust accumulation are near 0.4–0.5%/sol. ... However after sol 20, the power



Figure 12. Prominent clouds are seen in this InSight Instrument Context Camera (ICC) image acquired at 19:01 LMST, 30 min after sunset, on Sol 145. Image identifier C000M0145_609423773EDR_F0000_0516M1.PNG.

losses associated with dust accumulation on the lander solar panels fell below 0.1%/sol. ... It is interesting to note that the first dust devil was detected by the MPF Atmospheric Structure/Meteorology instrument on sol 25.”

The integrated energy from the solar arrays over the course of a day is an important operations consideration (e.g., Lisano & Kallemeyn, 2017), influencing the measurement activities and amount of data that can be returned to Earth. For operations purposes, this is estimated from an analytic function fit (cosine plus Gaussian) to combined array current and voltage information (the latter depending somewhat on temperature), and the integral under the fitted curve yields the energy budget. This daily energy production is shown in Figure 4 and follows essentially the same evolution as the peak current data. The energy output of the first InSight sol, some 4.6 kWh, is presently a record for the Martian surface and will likely remain so for several years.

4. Short-Term Solar Flux Variations

4.1. Dust Variations

Subtracting a smooth model fit from the instantaneous current values exposes (e.g., Figure 5) brief fluctuations in current that indicate changes in incident sunlight that have not been previously documented in detail. The $\sim 0.1\%$ resolution of the data and coherence of variation indicate these are real changes in solar flux, with the $\sim 1\%$ changes on timescales of a couple of hundred seconds to $\sim 1,000$ s likely due to ambient dust changes or thin clouds. While slight “flapping” of the arrays in the wind could lead to small current changes due to tilting, this would vary on subsecond timescales and so cannot be responsible for the coherent evolution on timescales of minutes to tens of minutes.

In the limit, single- or few-sample drops could be dust devil plumes (see the next section). However, the coherent and small variations seen here on 100- to 1,000-s timescales are likely the difference between dustiness of upwelling sheets and downwelling cells (e.g., Michaels & Rafkin, 2004) in the convecting planetary boundary layer (PBL), with upwellings presumably more dusty.

Renno et al. (2004) noticed a similar periodicity in ground heat flux measurements during a dust devil survey in Arizona but attributed it to a kind of dust-convection feedback where lofted dust reduces the solar input on the ground, resulting in less dust lifting, and so on. However, little other evidence for such a feedback exists, and since regularity in the Martian PBL has already been noted in the spacing of dust devils (Fenton & Lorenz, 2015), and the cellular structure of the PBL is evident in large-eddy simulations (e.g., Spiga et al., 2018), this is our preferred explanation. With a cellular pattern with a characteristic wavelength of the order of the PBL thickness (2–10 km) and advection speeds of the order of 5–10 m/s, quasiperiodic variations in other meteorological properties with periods of a few hundred seconds might be expected and indeed have been observed in the Viking windspeed and seismometer record (Lorenz et al., 2017). On the other hand, higher-altitude clouds of CO_2 or H_2O not infrequently have opacities (measured in camera images from the Curiosity rover—e.g., Kloos et al., 2018) of a few percent and, although typically more prominent in the early morning or late afternoon, can occur at all times of day.

Table 1
Phobos Eclipse Detections in Solar Array Data

Sol	Time (s)	Time (UT)	SA-771 (A)	SA-791 (A)	Drop (%)	Drop (%)
96	51,420.446	2019-03-05T10:48:14.294	0.21041	0.21743	11.8	11.8
98	44,592.912	2019-03-06T09:34:02.375	0.22152	0.21606	13.6	13.8
99	61,661.017	2019-03-08T15:37:41.719	0.06162	0.07741	3.1	2.2

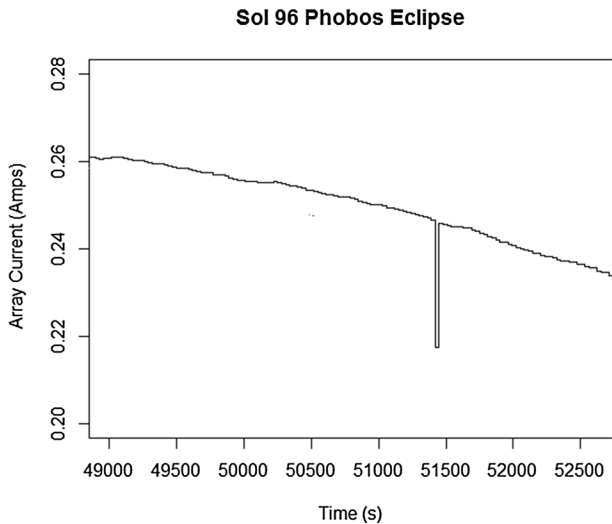


Figure 13. SA771 array current on Sol 96, showing the significant single-sample dip due to the Phobos shadow.

The vigor of these short-term variations can be calculated throughout the mission and expressed as a root-mean-square variation. It can be seen (Figure 6) that the deviations were strongest in the first 50 sols, intermediate in amplitude over Sols 70–170, and small outside those periods (e.g., during the dust storm), presumably indicating an evolution of dust and/or cloud activity.

4.2. Dust Devil Shadows

As previous Mars landers, InSight has detected many convective vortices as transient pressure drops. On Earth, the presence of dust in such vortices, making them “dust devils,” is detectable as a shadowing drop in solar flux in about 60% of pressure drops at the El Dorado site in Nevada (Lorenz & Jackson, 2015). We may recall that in fact the first dust devil reported by the Pathfinder lander as a pressure drop was accompanied (Schofield et al., 1997) by a drop in solar array current. Unfortunately, no further solar array data were reported in this context.

The 40% fraction requires some comment: If all vortices contain lofted dust, and measurements are conducted with the Sun directly overhead, only encounters where the “wall” of the dust devil (or perhaps some wider area of detrained dust at the top of the vortex column) will cause a shadow on a lander-mounted solar cell. If, in the more general case, the Sun is not at zenith, then a shadow is cast in the anti-Sun azimuth: With random dust devil paths, about half of near encounters would cause a shadow on the lander, and half would not. The actual detection of a shadow in some data set depends on both the detection threshold (Lorenz & Jackson, 2015, report about 60% of pressure-detected vortices had shadows of 0.1% or deeper, 40% were 1% or deeper, and 10% had more than 10% attenuation) and on the sampling frequency (pressure data were at two samples per second, solar flux at one sample per second). Clearly, if the shadow lasts only 10 s, then solar flux sampled at 60-s intervals has only a ~16% chance of detecting it.

A robust determination of upper limits on dust loading will require further analysis, likely with a Monte Carlo analysis taking time of day, advection speed, and other factors into account to estimate the detection efficiency, but suffice it to say at this point that at most a handful of vortices (e.g., Figure 7) have detectable shadows—consistent with the lack of reported detections of visible dust devils in InSight camera images. Most vortices at the InSight landing site are apparently dustless. This poses an interesting paradox, given that dust devil tracks have been observed to be generated there during the mission (Perrin et al., 2019) and previously (Reiss & Lorenz, 2016), so at least some dust-lifting must occur.

4.3. Clearing Event

Operational experience with the Mars Exploration Rovers indicated substantial, and essentially instantaneous, reductions in dust obscuration of the solar panels (Stella et al., 2009). In particular, within a 2-min period (data were acquired once per minute) around 11.57 a.m. on Sol 1899 of the Spirit rover mission, the solar array current increased by some 67%, restoring the “dust factor” to a value (0.6755) not seen since 630 sols previously. Stella et al. (2009) also noted that the array current data point at 11.56 a.m. was appreciably below the prior or subsequent values and speculated that this might have been due to the shadow of the dust devil during its passage.

Lorenz and Reiss (2015) reviewed the limited public data on the Spirit rover solar array dust factor history and noted that cleaning events occurred at the onset of the “dust devil season” (i.e., when dust devils were observed in camera images). They furthermore suggested that the frequency of cleaning events (once every few hundred sols) was consistent with encounters of vortices with pressure drops larger than some value

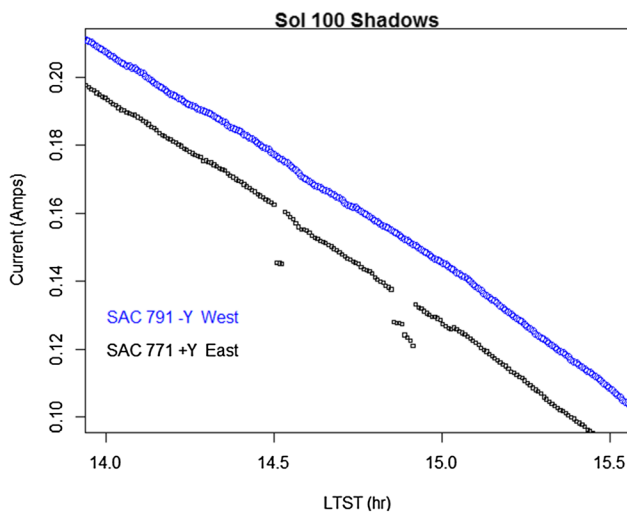


Figure 14. Array current histories on Sol 100. Two dips in the East array (SA0771) are seen—their “square-wave” shape betrays their artificial origin. The shadow seen in the image in Figure 1 corresponds to the 14.9 LTST dip. No such dip is seen in the other array (SA0791).

in the range 6–40 Pa. Vicente-Retortillo et al. (2018) studied dust correction factors on the ultraviolet flux sensors on the Curiosity rover and found that at that site (Gale crater, 4.6°S, not far from InSight) dust removal by convective vortices and nighttime winds tended to occur around perihelion, until $L_s \sim 300^\circ$, while dust tended to accumulate until the end of the aphelion season ($L_s \sim 180^\circ$). The vortex activity at Gale, and its dependence on the meteorological setting, has recently been documented by Newman et al. (2019).

Although vortex activity at InSight has been abundant (e.g., Banerdt et al., 2020; Banfield et al., 2020), no large cleaning events have been observed on InSight. However, a small cleaning was detected (Figure 8) at 14:52 UTC on 1 February 2019. This corresponds to 13:33 local true solar time (LTST) on Mars on Sol 65 of the InSight mission. On both Mars and Earth, the highest levels of dust devil activity are usually seen between about noon and 3 p.m., when the intensity of sunlight is strongest and the ground is hot compared with the air above it.

The wind direction measurements showed that the wind veered by about 180° during the event, which is typical when a strong dust devil passes straight over the observer. The highest wind speed recorded by the InSight TWINS wind measurements during the event was 17 m/s, but in fact the strongest winds in the event were not recorded because of the very rapidly varying turbulent speed and direction.

Just before the dust-cleaning event, the pressure reading was about 702 Pa: During the event the pressure dropped by over 9 Pa, or about 13%—possibly the largest vortex pressure drop detected on Mars so far.

Laboratory measurements (e.g., Neakrase & Greeley, 2010) show that a vortex with a pressure drop of 20–30 Pa can remove a monolayer of dust at Mars conditions in about 1 s from a flat metal surface. Those laboratory conditions with very small diameter vortices may not exactly replicate the adhesion of dust to solar panels on Mars and its removal by much larger vortices (probably in this case many tens of meters across), but they seem consistent with a 9-Pa vortex being able to provide at least some cleaning.

The wind stress on any individual part of the array may depend on the airflow around adjacent structures, notably the ribs used to stretch the folding arrays in their deployed condition. It is seen in Figure 9 that a localized streak of dust removal associated with the Sol 65 event could be observed apparently in the lee of one of these ribs. In fact, the total energy per sol did not change appreciably, so it may be that the dust removal was limited to the peripheral parts of the panel where the SAC-0791 and SAC-0771 currents were generated.

5. Twilight

As on Earth, the Martian sky does not become black at sunset, but scattering in the atmosphere causes the sky to have appreciable brightness with the Sun several degrees below the horizon. This twilight was observed with the Viking cameras (e.g., Kahn et al., 1981; Pollack et al., 1977). In fact, we find that the solar array current measurement is sensitive enough to pick up this effect with the Sun about 3° below the horizon (at low latitude, sunset and after sunrise occur nominally at 18:00 and 06:00 LTST, with the Sun rising or setting at a rate of 1° per 4 min)—see Figure 10.

This might be expected as a result of the abundant dust in the atmosphere, although, in principle, that should be a symmetric effect at both dawn and dusk. That said, there are small optical depth variations with time of day (e.g., Pollack et al., 1977).

In fact, the evolution of the postsunset array current (data taken at 18:12 LTST, with the Sun nominally 3° below the horizon) has a highly nonmonotonic behavior (Figure 11a, bottom point cloud). There is apparently a suspended dust signal between about Sol 45 and 60, corresponding with the peak optical depth of the dust storm as measured by the InSight cameras, but even more striking is the frequent occurrence of 1- to 2-mA currents (corresponding to light levels about 1% of those near noon) after Sol 100. There is no corresponding sunrise effect.

It seems likely that these twilight currents are caused by light scattering by noctilucent clouds—water or CO_2 ice clouds that are high enough to be directly illuminated by the Sun (see, e.g., Clancy et al., 2003; Määttä et al., 2013). Indeed, such clouds have been visible in camera images acquired in sunset and postsunset imaging campaigns after Sol 140—Figure 12 shows one example. In their discussion of prelanding

meteorological expectations, Spiga et al. (2018) noted that InSight is at low enough latitude to be in the Mars aphelion cloud belt, and orbital observations cited there support the expectation of visible clouds forming from about $L_s = 0^\circ$ (InSight Sol 117) and increasing up to northern summer solstice ($L_s = 90^\circ$, InSight Sol 320).

Clouds during the day could of course be detected as transient or sustained dips in recorded current and are regularly observed on Earth in similar data (e.g., Harrison et al., 2008; Lorenz & Jackson, 2015). However, while nonimaging red/blue flux comparisons can allow cloud identification (e.g., Toledo et al., 2016), it is impossible with broadband solar array data to discriminate clouds (of water or CO₂ ice at high altitude) from dust variations in the lower atmosphere as discussed in section 4.1.

6. Phobos Shadow

Midway in the operations period reported in this paper, the shadow of Phobos was predicted to pass over the InSight lander. The brief shadow passages were detected in the solar array current data on all three days (Table 1), but only as single-sample dips in array current (Figure 13), so in this instance the data are of limited utility in ephemeris refinement or other analyses. The low amplitude of the Sol 99 dip is consistent with a grazing (partial) eclipse.

7. Lander Operations

Although spacecraft operations are usually deterministic and there is little to discover in these data, it is worth pointing out operations' influence, so that their signature is not mistaken for other environmental effects.

Operations on a spacecraft are typically diagnosed by monitoring power supply currents (e.g., a motor being commanded on may draw more current). The solar array current here does not correspond to any commands, since the cells are wired directly to the battery. However, spacecraft operations can influence the current if they lead to a change in light falling on the array—such an occasion occurred on Sol 100 (Figure 14). Brief current dips were investigated initially as being possible dust devil shadows, but their appearance on only one array, their sudden onset, and near-constant attenuation argued against such an origin, and so shadow by the robot arm was suspected. Inspection of the image archive not only showed that the arm was in a position that might cause a shadow but in fact (see Figure 1) showed the shadow itself.

8. Conclusions

Nonimaging sensors to perform monitoring of optical fluxes at the Martian surface have been proposed previously (e.g., Maria et al., 2006; Toledo et al., 2016) and indeed flown (Towner et al., 2004; Gómez-Elvira et al., 2012; Smith et al., 2016). However, despite the lack of collimation or wavelength selectivity, the solar array current measurements on a Mars lander, even at the low sampling rate required for engineering evaluation of mission energy budgets, provide useful situational awareness of the dust and cloud environments, including previously unreported opacity variations in the planetary boundary layer. The record from the first 200 sols of InSight operation yields a useful new window on meteorological processes as well as on spacecraft operations, and these encouraging results have motivated an increase in the sample rate of these data. It is urged that solar array data from other missions be similarly made available for scientific exploitation.

References

- Banerdt, W. B., Smrekar, S., Banfield, D., Giardini, D., Golombek, M., Johnson, C., et al. (2020). Early results from the InSight mission: Mission overview and global seismic activity. *Nature Geoscience*, *13*(3), 183–189. <https://doi.org/10.1038/s41561-020-0544-y>
- Banfield, D., Spiga, A., Newman, C., Forget, F., Lemmon, M., Lorenz, R., et al. (2020). The atmosphere of Mars as observed by InSight. *Nature Geoscience*, *13*(3), 190–198. <https://doi.org/10.1038/s41561-020-0534-0>
- Clancy, R. T., Wolff, M. J., & Christensen, P. R. (2003). Mars aerosol studies with the MGS TES emission phase function observations: Optical depths, particle sizes, and ice cloud types versus latitude and solar longitude. *Journal of Geophysical Research*, *108*(E9), 5098. <https://doi.org/10.1029/2003JE002058>
- Coyne, J., Jackson, W. and Lewicki, C., 2009, August. Phoenix electrical power subsystem-power at the Martian pole. In 7th International Energy Conversion Engineering Conference (p. 4518). <https://arc.aiaa.org/doi/pdf/10.2514/6.2009-4518>
- Crisp, D., Pathare, A., & Ewell, R. C. (2004). The performance of gallium arsenide/germanium solar cells at the Martian surface. *Acta Astronautica*, *54*(2), 83–101.

Acknowledgments

R. L. acknowledges the support of the NASA InSight Participating Scientist Program via grant 80NSSC18K1626. A. S. acknowledges the support of the Centre National d'Etudes Spatiales (CNES). We thank Mike Lisano and Dhack Muthulingham for useful insights on the architecture of the InSight solar arrays and Brian Carcich for streamlining the availability of solar array data within the team via the Mars Weather Service (MWS). The InSight solar array data are available on the NASA Planetary Data System (PDS) in the InSight Spacecraft Raw Engineering and Ancillary Data Collection in the InSight-IFG-Mars bundle held at the Planetary Plasma Interactions PDS Node (<https://pds-ppi.igpp.ucla.edu>). A simplified product, containing only array current and timing information, is archived at the Johns Hopkins Applied Physics Laboratory Data Archive site (<http://lib.jhuapl.edu/>). InSight imaging data are at the PDS imaging node (https://pds-imaging.jpl.nasa.gov/data/nsyt/insight_cameras/). This publication is InSight contribution 109.

- Fenton, L. K., & Lorenz, R. (2015). Dust devil height and spacing with relation to the Martian planetary boundary layer thickness. *Icarus*, 260, 246–262.
- Gómez-Elvira, J., Armiens, C., Castañer, L., Domínguez, M., Genzer, M., Gómez, F., et al. (2012). REMS: The environmental sensor suite for the Mars science laboratory rover. *Space Science Reviews*, 170(1–4), 583–640.
- Harrison, R. G., Chalmers, N., & Hogan, R. J. (2008). Retrospective cloud determinations from surface solar radiation measurements. *Atmospheric Research*, 90(1), 54–62.
- Kahn, R., Goody, R., & Pollack, J. (1981). The Martian twilight. *Journal of Geophysical Research*, 86(A7), 5833–5838.
- Kloos, J. L., Moores, J. E., Lemmon, M., Kass, D., Francis, R., De La Torre Juárez, M., et al. (2016). The first Martian year of cloud activity from Mars Science Laboratory (sol 0–800). *Advances in Space Research*, 57(5), 1223–1240.
- Kloos, J. L., Moores, J. E., Whiteway, J. A., & Aggarwal, M. (2018). Interannual and diurnal variability in water ice clouds observed from MSL over two Martian years. *Journal of Geophysical Research: Planets*, 123, 233–245. <https://doi.org/10.1002/2017JE005314>
- Lam, G. Q., Billets, S., Norick, T. and Warwick, R., 2016. Solar array design for the Mars InSight lander mission. In 14th International Energy Conversion Engineering Conference, July 25–27, 2016, Salt Lake City, UT. AIAA-2016-4520. Doi: <https://doi.org/10.2514/6.2016-4520>
- Landis, G. A. (1996). Dust obscuration of Mars solar arrays. *Acta Astronautica*, 38(11), 885–891.
- Lemmon, M. T., Wolff, M. J., Bell, J. F. III, Smith, M. D., Cantor, B. A., & Smith, P. H. (2015). Dust aerosol, clouds, and the atmospheric optical depth record over 5 Mars years of the Mars exploration rover mission. *Icarus*, 251, 96–111.
- Lisano, M. E. and Bernard, D., 2014, March. An almanac of Martian dust storms for InSight project energy system design. In 2014 IEEE Aerospace Conference, Big Sky, MT March 2014. <https://doi.org/10.1109/AERO.2014.6836269>
- Lisano, M.E. and Kallemeyn, P.H., 2017, March. Energy management operations for the InSight solar-powered mission at Mars. In 2017 IEEE Aerospace Conference, Big Sky, MT March 2017. <https://doi.org/10.1109/AERO.2017.7943965>
- Lorenz, R. D., & Jackson, B. K. (2015). Dust devils and dustless vortices on a desert playa observed with surface pressure and solar flux logging. *GeoResJ*, 5, 1–11.
- Lorenz, R. D., Nakamura, Y., & Murphy, J. R. (2017). Viking-2 seismometer measurements on Mars: PDS data archive and meteorological applications. *Earth and Space Science*, 4(11), 681–688.
- Lorenz, R. D., & Reiss, D. (2015). Solar panel clearing events, dust devil tracks, and in-situ vortex detections on Mars. *Icarus*, 248, 162–164. <https://doi.org/10.1016/j.icarus.2014.10.034>
- Maria, J. L., Tran, T. T., Pommereau, J. P., Rannou, P., Malique, C., Correia, J. J., & Porteneuve, J., (2006). Technical aspect of the optical depth sensor. *Advances in Space Research*, 38(4), 726–729.
- Määttä, A., Pérot, K., Montmessin, F., & Hauchecorne, A. (2013). Mesospheric clouds on Mars and on Earth. In S. Mackwell, A. Simon-Miller, A. Harder, & M. Bullock (Eds.), *Comparative climatology of terrestrial planets*, (pp. 393–413). Arizona: University of Arizona Press.
- Michaels, T. I., & Rafkin, S. C. (2004). Large-eddy simulation of atmospheric convection on Mars. *Quarterly Journal of the Royal Meteorological Society*, 130(599), 1251–1274.
- Neakrase, L. D., & Greeley, R. (2010). Dust devil sediment flux on Earth and Mars: Laboratory simulations. *Icarus*, 206(1), 306–318.
- Newman, C. E., Kahanpää, H., Richardson, M. I., Martínez, G., Vicente-Retortillo, Á., & Lemmon, M. (2019). Convective vortex and dust devil predictions for Gale crater over three Mars years and comparison with MSL-REMS observations. *Journal of Geophysical Research: Planets*, 124, 3442–3345. <https://doi.org/10.1029/2019JE006082>
- Perrin, C., S. Rodriguez, A. Jacob*, A. Lucas, B. Kenda, A. Spiga, et al., Searching for geological surface changes around the InSight landing site (Mars) from HiRISE satellite images. Abstract #2390, 50th Lunar and Planetary Science Conference 2019 (LPI Contrib. No. 2132), Houston, March 2019
- Pollack, J. B., Colburn, D., Kahn, R., Hunter, J., Van Camp, W., Carlston, C. E., & Wolf, M. R. (1977). Properties of aerosols in the Martian atmosphere, as inferred from Viking Lander imaging data. *Journal of Geophysical Research*, 82(28), 4479–4496.
- Rapp, D. 2004. Solar energy on Mars: Volume 1. Basics, JPL D-21342-Vol. 1 Jet Propulsion Laboratory, December 2004
- Reiss, D., & Lorenz, R. (2016). Dust devil track survey at Elysium Planitia, Mars: Implications for the InSight landing sites. *Icarus*, 266, 315–330.
- Renno, N. O., Abreu, V. J., Koch, J., Smith, P. H., Hartogensis, O. K., De Bruin, H. A., et al. (2004). MATADOR 2002: A pilot field experiment on convective plumes and dust devils. *Journal of Geophysical Research: Planets*, 109(E7), E07001. <https://doi.org/10.1029/2003JE002219>
- Sayyah, A., Horenstein, M. N., & Mazumder, M. K. (2014). Energy yield loss caused by dust deposition on photovoltaic panels. *Solar Energy*, 107, 576–604.
- Schofield, J. T., Barnes, J. R., Crisp, D., Haberle, R. M., Larsen, S., Magalhaes, J. A., et al. (1997). The Mars Pathfinder atmospheric structure investigation/meteorology (ASI/MET) experiment. *Science*, 278(5344), 1752–1758. <https://doi.org/10.1126/science.278.5344.1752>
- Smith, M. D., Zorzano, M. P., Lemmon, M., Martín-Torres, J., & de Cal, T. M. (2016). Aerosol optical depth as observed by the Mars science laboratory REMS UV photodiodes. *Icarus*, 280, 234–248.
- Spagnuolo, M. G., Carballo, F. D., Marco Figuera, R., & Rossi, A. P. (2019). MarsLux: HI-resolution illumination maps generator for Mars. *Earth and Space Science*, 6(1), 146–155. <https://doi.org/10.1029/2018EA000403>
- Spiga, A., Banfield, D., Teanby, N. A., Forget, F., Lucas, A., Kenda, B., et al. (2018). Atmospheric science with InSight. *Space Science Reviews*, 214(7), 109.
- Stella, P.M., Chin, K., Wood, E., Herman, J. and Ewell, R., 2009, June. Managing PV power on Mars—MER rovers. In 2009 34th IEEE Photovoltaic Specialists Conference (PVSC) (pp. 001073-001078). IEEE. doi:<https://doi.org/10.1109/PVSC.2009.5411206>
- Stella, P.M., Mardesich, N., Edmondson, K., Fetzler, C. and Boca, A., 2008, May. Mars optimized solar cell technology (MOST). In 2008 33rd IEEE Photovoltaic Specialists Conference (pp. 1-6). IEEE. <https://doi.org/10.1109/PVSC.2008.4922711>
- Toledo, D., Rannou, P., Pommereau, J.-P., Sarkissian, A., & Foujols, T. (2016). Measurement of aerosol optical depth and sub-visual cloud detection using the optical depth sensor (ODS). *Atmospheric Measurement Techniques*, 9(2), 455–467.
- Towner, M. C., Patel, M. R., Ringrose, T. J., Zarnecki, J. C., Pullan, D., Sims, M. R., et al. (2004). The Beagle 2 environmental sensors: Science goals and instrument description. *Planetary and Space Science*, 52(13), 1141–1156.
- Vicente-Retortillo, Á., Martínez, G. M., Renno, N., Newman, C. E., Ordóñez-Etxeberria, I., Lemmon, M. T., et al. (2018). Seasonal deposition and lifting of dust on Mars as observed by the Curiosity rover. *Scientific Reports*, 8(1), 1–8. <https://doi.org/10.1038/s41598-018-35946-8>